JOURNAL OF GEOPHYSICAL RESEARCH, VOL. 106, NO. C4, PAGES 7001–7015, APRIL 15, 2001

Asymmetry in the response of a stratified coastal embayment to wind forcing

Fraser J.M. Davidson, [1] Richard J. Greatbatch,[2] and Brad de Young

Department of Physics and Physical Oceanography, Memorial University of Newfoundland, St. John's, Canada

Abstract. We investigate mechanisms that lead to asymmetry in the response of a stratified coastal embayment following the onset of a uniform, steady wind that is blowing both along the axis and out of the bay. We focus on bays on the east coast of Newfoundland where the typical duration of wind events is 5 days and stratification representative of June conditions yields a first baroclinic mode wave speed of 0.51 m s^{-1}. We use several numerical models ranging from a linear, reduced gravity model with a single baroclinic mode, to a nonlinear, prognostic, primitive equation model (CANDIE). We investigate the effect of factors such as continuous stratification, vertical mixing, nonlinearity, and realistic bottom topography. If the linear dynamics of only the first baroclinic mode is considered, the response of the idealized bay to 5 days of steady wind forcing is symmetric about the axis of the bay. Continuous stratification allows for higher-order vertical modes. These slower modes increase the response time of the bay, yielding asymmetry in the circulation pattern after 5 days of constant wind forcing. Model results using realistic geometry demonstrate that realistic bottom topography has little effect on near-surface circulation on the 5 day timescale. Adding nonlinearity allows a significant cross-bay transport of upwelled water and leads to the characteristic along-bay pattern of the surface isotherms evident in observations and can also lead to the separation of the coastal jet from the upwelling favorable shore.

1. Introduction

Conception Bay is roughly 30 km wide and 70 km long on the east coast of Newfoundland, Canada. It reaches a depth of 200 m with stratification in the top 70 m strengthening throughout the summer and early fall. Below 70 m, stratification is weak and constant throughout the summer. The prevailing wind during the summer is from the southwest, manifested as periods of wind blowing out of the bay for roughly 5 days at a time [*de Young et al.*, 1993].

A common observation in Conception Bay, and also neighboring Trinity Bay immediately to the northwest, is that the western side of the bay is cooler than the eastern side, even after several days of wind blowing out of the bay. This is evident from local experience and satellite-based sea surface temperature observations (Figure 1). Furthermore, mooring observations [*de Young et al.*, 1993] suggest that upwelling events are weaker on the eastern side of the bay than on the western side. Simple wind forced, shallow-water models with one baroclinic mode do not reproduce the preponderance for upwelling on the west side over the east side of the bay [*de Young et al.*, 1993].

An idealized bay can be represented as a series of four right angle corners along an infinite straight coastline. Coastal trapped waves propagate around the bay leaving along-shore and cross-shore pressure gradients in their wake [*Gill*, 1982; *Crepon et al.*, 1984]. These waves are responsible for establishing the pressure gradient and the tilting of the thermocline in the bay in response to wind forcing. The adjustment time is determined by the wave propagation speed and coastline length. For wind blowing straight out of an idealized 40 km square bay, with neither mixing or damping, *Greatbatch and Otterson* [1991] ran a single-layer, reduced gravity model and found that the steady state horizontal pressure field set up by the passage of baroclinic Kelvin waves is symmetric about the axis of the bay. Outside the bay, the flow is in Ekman balance. Inside the bay, the flow is pressure driven within a Rossby radius (5 km) of the coast, leading to an anticyclonic gyre governed by geostrophy near the coast and wind driven Ekman drift over the interior.

[1] Now at Laboratoire d'Etudes en Geophysique et Oceanographie Spatiales, LEGOS/GRGS, Toulouse, France.

[2] Now at Department of Oceanography, Dalhousie University, Halifax, Nova Scotia, Canada.

Paper number 2000JC900052.
0148-0227/01/2000JC900052$09.00

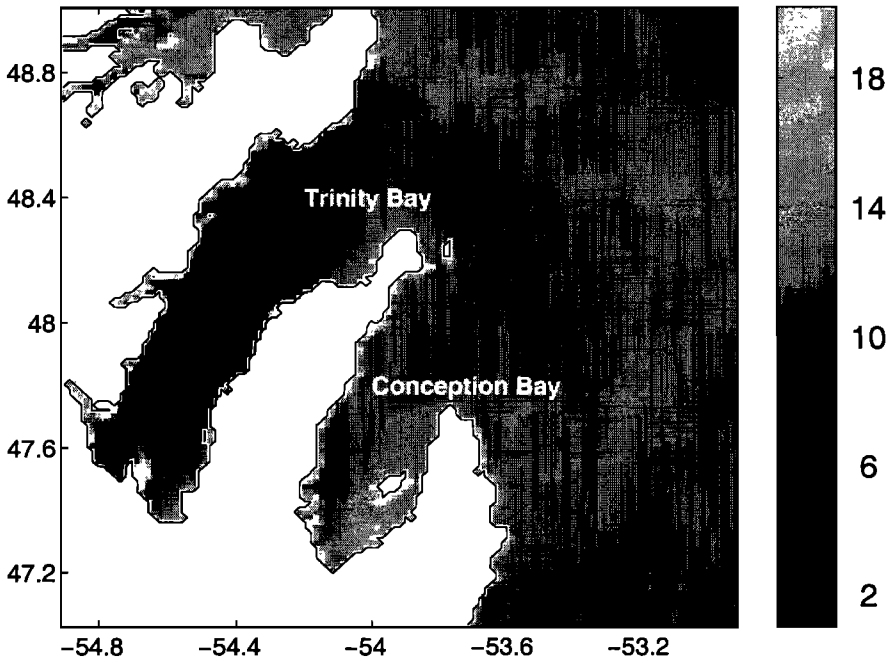

Figure 1. Observed sea surface temperature (°C) in Conception and Trinity Bays on August 4, 1997. The black line represents the 4°C isotherm. The northwest side of both bays are significantly cooler than the southeast side. Wind has been blowing from the southwest for the previous 3-4 days. The picture is based on an Advance Very High Resolution Radiometer satellite image (Courtesy of Peter Cornillion, University of Rhode Island) and processed using the Rosenstiel School of Marine and Atmospheric Science sea surface temperature algorithm.

When continuous stratification is taken into account, the adjustment no longer involves just a single baroclinic mode but also higher modes with more complex vertical structure and slower propagation speeds. The adjustment time for these higher modes may be longer than the typical duration of wind events (5 days for Conception Bay), leading to an asymmetry in the response of the bay to wind events. In addition waves may also be dissipated by mixing before leaving the bay, and variable bottom topography can lead to wave scattering [*Killworth*, 1977; *Wilkin and Chapman*, 1990], mechanisms that can also lead to an incomplete adjustment and hence asymmetry.

If the coefficients for the vertical mixing of momentum (ν) and density (κ) are assumed proportional to $1/N^2$ (where N is the Brunt-Väisälä frequency), the linear equations of motion for a flat-bottomed ocean can be reduced, using standard vertical normal modes, to a set of shallow water equations for each mode [*McCreary*, 1981]. Vertical mixing of momentum is then represented by Rayleigh friction and vertical mixing of density by a Newtonian damping term. These linear damping coefficients vary as $1/c_n^2$ where c_n is the wave speed of each mode. For equal vertical mixing of momentum and density, the distance traveled by a wave before being damped by a factor 1/e is therefore proportional to c_n^3. Higher vertical mode waves, for which c_n varies as $1/n$, are therefore much more efficiently damped than lower mode waves. Higher vertical modes are also associated with smaller horizontal and vertical spatial scales.

As the restoring force for internal Kelvin waves is gravity, diffusion of stratification rather than mixing of momentum is ultimately more effective in damping the waves [*Yamagata and Philander*, 1985]. The ratio of momentum over density mixing represented by

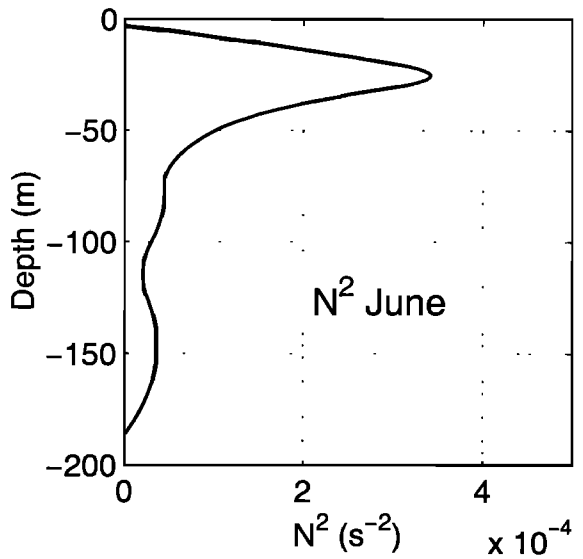

Figure 2. Profile of N^2 for the month of June. The 40 year average density structure was used.

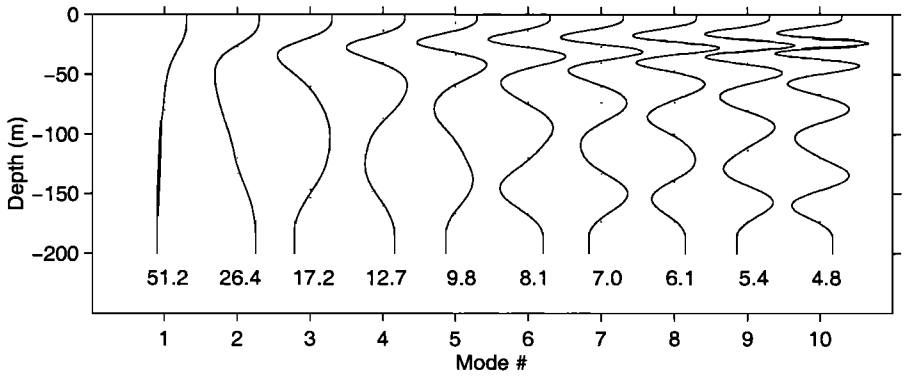

Figure 3. Modal structure of the first 10 baroclinic modes. Phase speeds (cm s^{-1}) are shown below each modal structure.

the Prandtl Number (Pr) changes the spatial scale of the response and the velocity amplitude [*Yamagata and Philander*, 1985].

This paper models the baroclinic response of an idealized coastal embayment to the onset of a steady uniform wind blowing out of the bay. We investigate the factors that affect the response of the bay and provide a cross-bay asymmetry after a 5 day period. These factors include continuous stratification, damping of waves through mixing of momentum and density, the effects of changing the Prandtl Number (Pr), the effects of variable bottom topography and variable coastline shape, and finally the effect of nonlinearity. We make use of numerical models of increasing complexity, from a linear, single-layer, reduced gravity model to a full three-dimensional (3-D) numerical model that includes all the nonlinear terms and realistic bottom topography.

This paper is presented as follows. In section 2, we describe the model setup. In section 3, we discuss the wind-forced response of shallow water models ranging from a single-layer, baroclinic model to a continuously stratified, flat-bottomed ocean model solved using the vertical normal modes approach of *McCreary* [1981]. In section 4, we apply the 3-D model known as CANDIE [*Sheng et al.*, 1998] and explore the effect of nonlinearity. In section 5, we use CANDIE to include the realistic coastline and bottom topography of Trinity and Conception Bays. In section 6, we present our discussion and conclusions. An appendix is included to summarize the numerical circulation models employed as well as the formulation of our open boundary conditions.

2. Model Setup

In this paper, three different models are used; a single-layer, reduced gravity model, a continuously stratified linear model (based on the method of *McCreary* [1981]), and a 3-D circulation model [*Sheng et al.*, 1998]. The details of each of these models are given in the appendix. This section describes the implementation of these models.

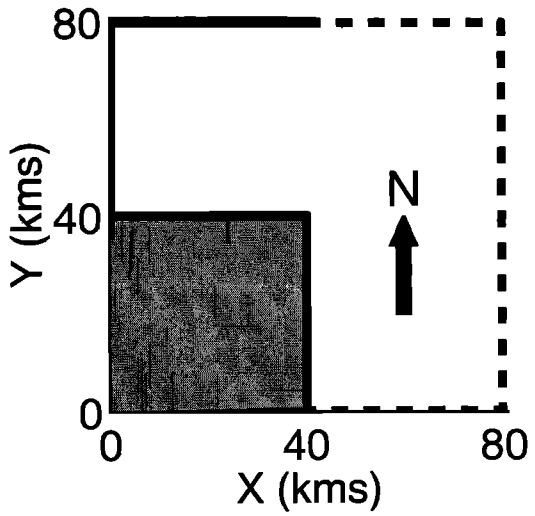

Figure 4. Idealized model topography of a square bay. Open boundaries of the domain are indicated by dashed lines. Solid lines indicate closed boundaries. Bottom depth is 200 m for the continuously stratified normal mode model.

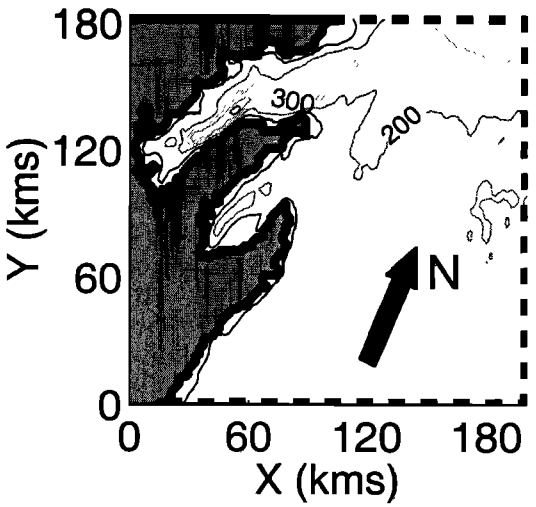

Figure 5. Model topography for Trinity and Conception Bays. Depth contours are every 100 m. Dashed lines indicate open boundaries.

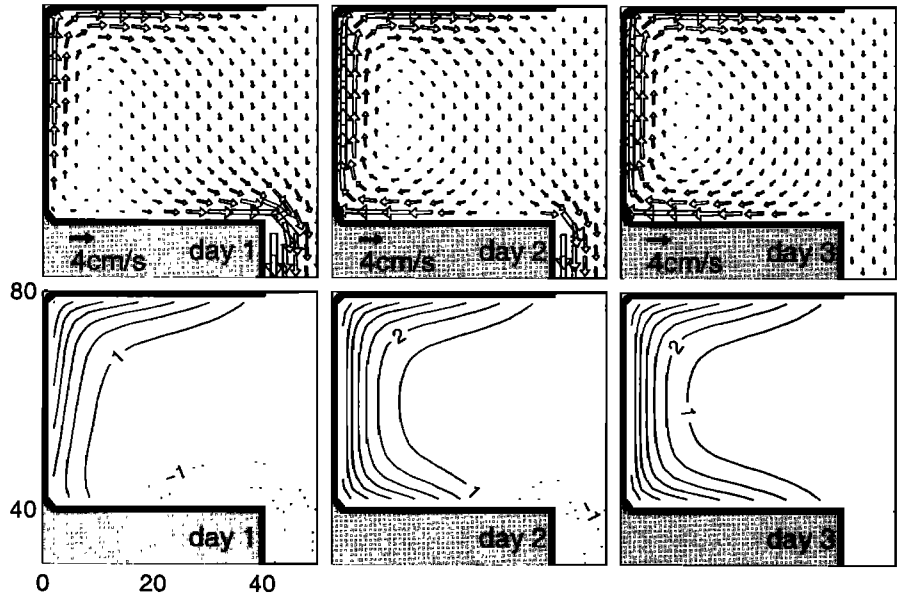

Figure 6. (top) Upper layer velocity from the single-layer, reduced-gravity model run with a phase speed $c = 0.5$ m s^{-1} and no damping (i.e., inviscid) at days 1, 2, and 3. (bottom) As in Figure 6, top, but for interface displacement. Solid lines represent upward interface displacement, and dotted lines represent downward interface displacement. The interval between contours is 1 m.

2.1. Stratification and Phase Speeds

We use observed June data from Station 27, situated 20 km from the mouth of Conception Bay, as a proxy for water density in Conception and Trinity Bays. The density profile at Station 27 is obtained from density observations at set depths of 0, 10, 20, 30, 50, 75, 100, 125, 150, and 175 m [*Petrie et al.*, 1992]. All density observations taken in the month of June over a 40 year observation period are used to extract an average density profile. We then calculate a representative vertical profile of N^2 (see Figure 2). Using the N^2 profile, we solve for the vertical mode functions and their respective phase speeds (Figure 3) assuming a uniform depth of 200 m. The rigid lid approximation is applied. The wave speed of the first baroclinic mode for the month of June is 0.51 m s^{-1}, implying a Rossby radius of deformation of 5 km. For the rest of the year, similarly calculated monthly phase speeds vary between $c_1 = 0.3$ m s^{-1} in March and $c_1 = 0.8$ m s^{-1} in September for the first baroclinic mode.

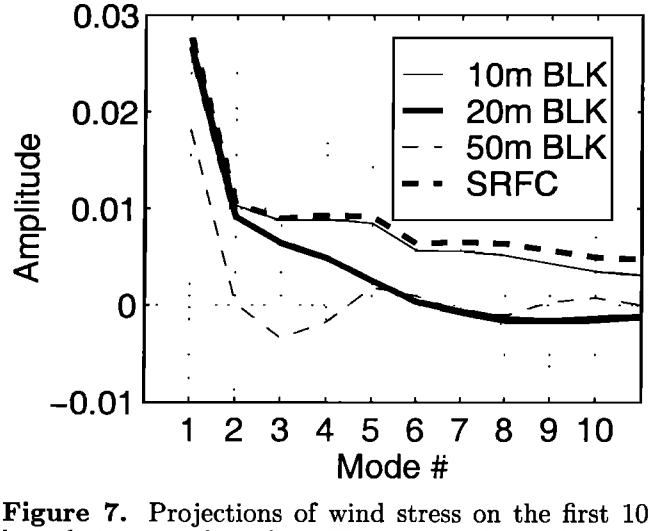

Figure 7. Projections of wind stress on the first 10 baroclinic normal modes. The amplitude of the projection determines the importance of each mode in the wind-driven response. The label BLK refers to treating the wind forcing as a body force. SRFC specifies the wind stress as a surface boundary condition. The 10 m body force and the surface wind stress methods resemble each other the most. Applying the wind over a deeper layer reduces the influence of higher modes.

2.2. Model Domain

We make use of two model geometries, an idealized square embayment (Figure 4) and the realistic coastline geometry of Trinity and Conception Bays (Figure 5). For those model runs that use a flat bottom, the depth is 200 m. We use the realistic bottom topography (Figure 5) for some of the runs using the 3-D model. Some runs use a single-layer, reduced gravity model as given by *Greatbatch and Otterson* [1991] and *de Young et al.* [1993]. In all cases, the model's upstream open boundary (in the sense of Kelvin wave propagation) is an extension of the northern coastline as given by *Greatbatch and Otterson* [1991]. The details of the boundary treatment at this and the other open boundaries are given in the appendix.

Hsieh et al. [1983] show that if the model horizontal grid spacing exceeds the Rossby radius of deformation,

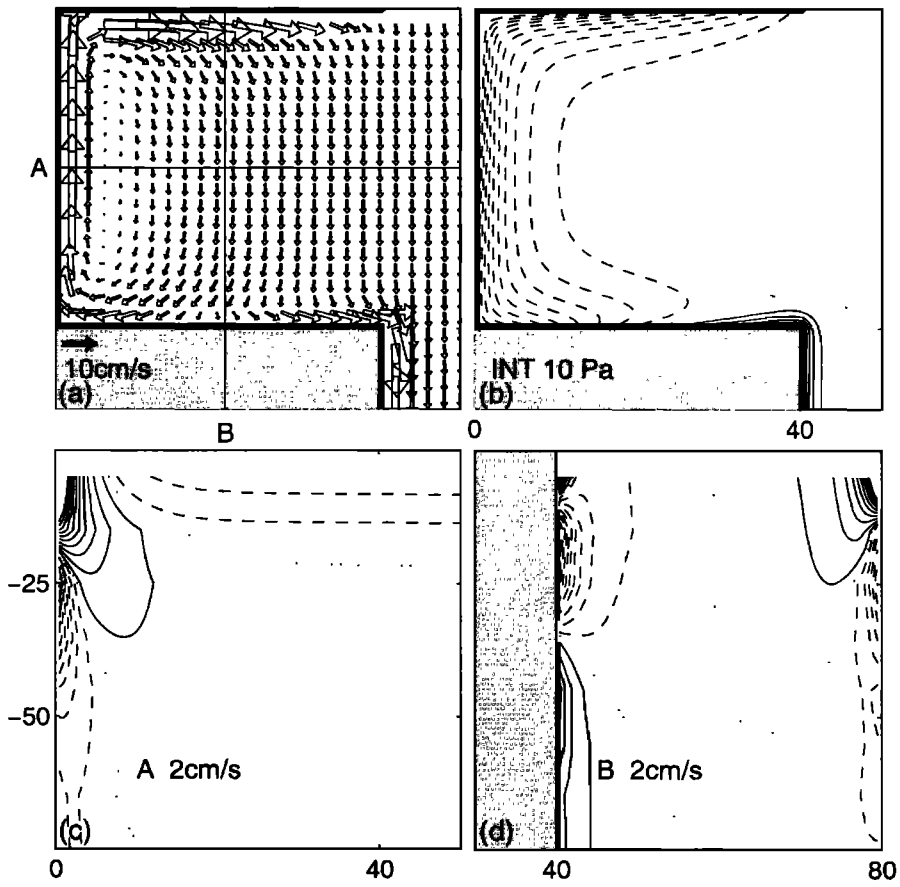

Figure 8. The normal mode model at day 5 with no friction or damping. (a) Surface velocity field. (b) Surface Pressure field with a contour interval of 10 Pa. Dashed contours represent negative pressure anomaly and solid lines indicate a positive pressure anomaly. (c) Vertical profile of velocity normal to transect A. (d) Vertical profile of velocity normal to transect B. The maximum depth shown in the vertical transect plots is 75 m. The contour interval is 2 cm s^{-1} with solid contours indicating flow into the page and dashed contours indicating flow out of the page. The zero contour is shown using a dotted line.

spurious spatial oscillations occur. The use of 500 m grid spacing ensures resolution of the radius of deformation for the first 10 baroclinic modes in Figure 3.

2.3. Model Initialization

Our primary objective is to investigate the response of a bay to a wind blowing steadily along the axis of the bay toward the mouth over a 5 day period. Models are initialized at rest with horizontally uniform stratification. In the reduced gravity model the initial upper layer depth is uniform at 40 m. For the normal mode model, the pressure anomaly for each mode is initially zero. In the 3-D model, the initial density stratification is specified using the averaged June profile. A wind stress of 0.05 Pa directed out of the bay is introduced over 2 days using a hyperbolic tangent ramping function. This smoothed application of wind stress avoids exciting near-inertial oscillations [*Pollard and Millard*, 1970]. We start measuring time when wind reaches 50% strength (i.e., after 1 day).

3. Shallow Water Model: Single Layer and Continuous Stratification

3.1. Methods

We begin by showing a result from the reduced gravity, shallow water model with the wave speed chosen to correspond to the first baroclinic mode. Velocities and interface displacement are shown in Figure 6 for a case with no friction or damping. For a wave speed of 0.5 m s^{-1}, Kelvin waves propagate roughly 40 km in a day. The model therefore reaches steady state by day 3, after which all Kelvin waves have left the domain and the interface displacement is symmetric about the axis of the bay.

The open-boundary condition is designed so that no waves may enter the domain through the northern boundary [*Greatbatch and Otterson*, 1991]. Figure 6 shows that the northern side of the bay is first to reach steady state. Kelvin waves are generated at the mouth and propagate along this boundary within a day. The last region to reach steady state is the downstream side

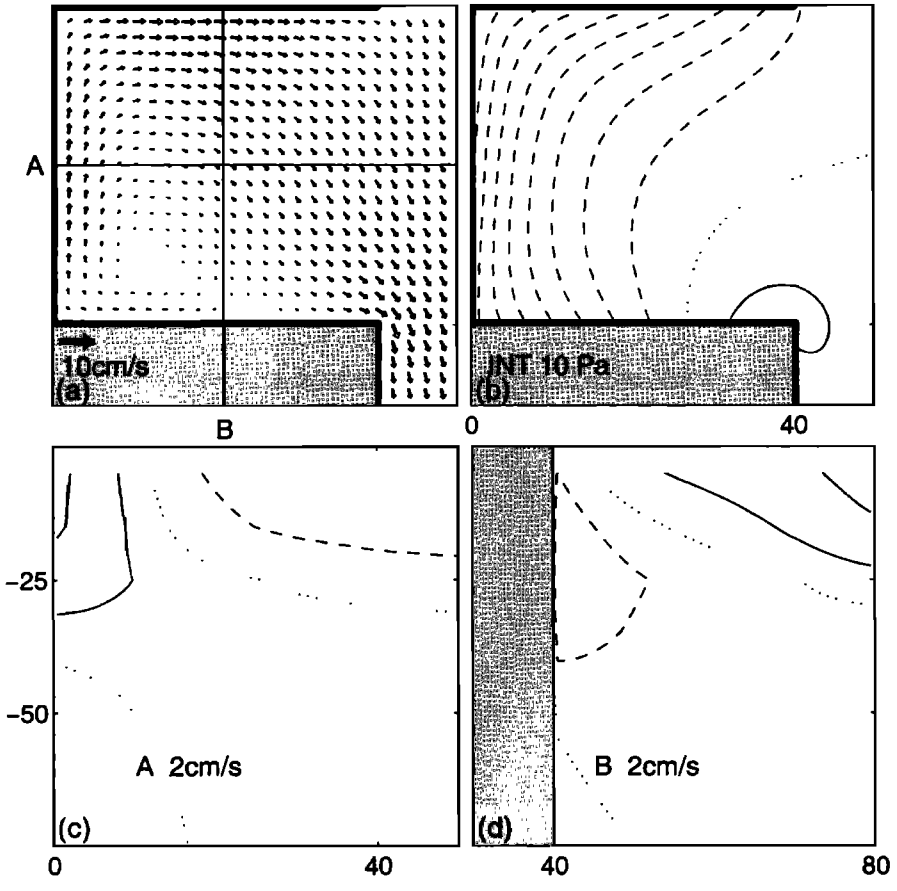

Figure 9. As in Figure 8 but with a Prandtl number of 100 (i.e., now $A_m = 2 \times 10^{-8}$ m^2 s^{-3}).

of the bay near the mouth, where Kelvin waves exit the bay.

Next we include continuous stratification with a finite bottom depth of 200 m. The solution procedure is described in the appendix but basically involves solving the finite difference shallow water equations for the first 10 baroclinic normal modes and then summing the modes to obtain the complete solution (summing over more than the first 10 modes does not significantly change the result). The inclusion of higher modes with slower propagation speeds leads to an asymmetry in the cross-bay structure after 5 days that is not found in Figure 6. The importance of the higher modes depends on the extent to which the wind forcing projects onto each mode.

We consider the two following methods of applying the wind stress to the water column: (1) as a surface boundary condition or (2) as a body force acting over a layer of depth H_M. Figure 7 shows the magnitude of the wind stress projection on the first 10 baroclinic modes for each of the two methods and for H_M = 10, 20, and 50 m. These projections determine the forcing function applied to the shallow water momentum equations associated with each mode. For a body force acting on a 10 m layer, the wind stress projection onto the first 10 modes is very similar to that obtained when the wind stress is applied as a surface boundary condition (given by (5) in the appendix). Effective wind forcing of modes higher than 2 is reduced for a body force distributed over a depth of 20 or 50 m.

3.2. Results

In the first set of simulations the model is run with the wind stress implemented as a body force acting over a depth of 10 m. As noted above, for the first ten modes, this gives a projection onto each mode very similar to that when the wind stress is implemented as a surface boundary condition. The model is first run with no friction or damping. Note that running the model with no vertical mixing of momentum yet implementing the wind forcing as a surface boundary condition makes no physical sense. The use of the 10 m body force approach corresponds to having very large vertical eddy viscosity in the top 10 m and zero vertical mixing of momentum below 10 m.

By day 5, the third mode and higher Kelvin waves have not exited the bay. This is apparent in the velocity and pressure field (Figure 8) along the south shore of the bay where there is outflow near the mouth. Also, the anticyclonic gyre is now restricted to the inner half

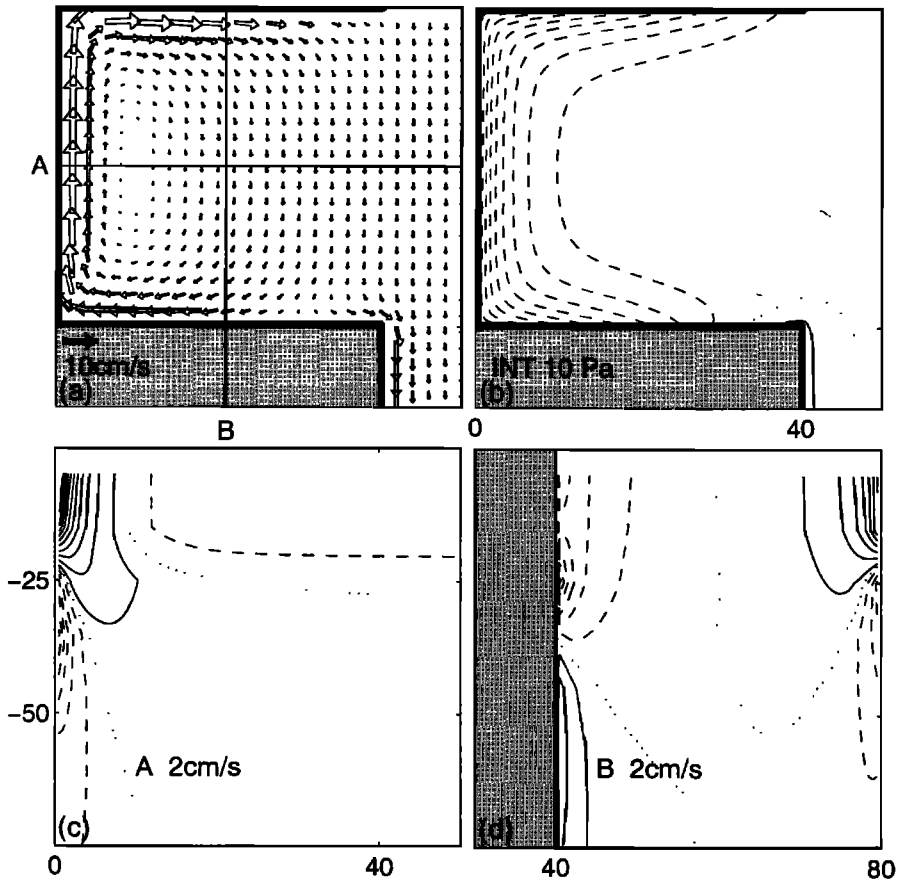

Figure 10. The normal mode model at day 5 as in Figure 8, but with wind stress modeled as a body force acting over the top 20 m.

of the bay, whereas in Figure 6 it fills the whole bay after only 3 days. We note that the interface displacement shown in Figure 6 is related to pressure in the single layer reduced gravity model by a negative constant. Thus we can compare the interface elevation pattern in Figure 6 with the surface pressure in Figure 8. The baroclinic flow structure of the coastal jet is clearly visible in the crosssections of currents shown in Figure 8. On transect A, the northward coastal surface jet at the head of the bay has reverse flow at depth and extends away from the coast below the wind driven Ekman current. On transect B, there is generally anticyclonic flow in the upper part of the water column, and cyclonic flow at depth, although the detailed vertical structure is different on the southern and northern boundaries due to the different contributions from the different normal modes. It is clear from these results that taking account of the realistic density stratification in the bay and the role played by the higher baroclinic normal modes is sufficient to lead to a significant asymmetry in the cross-bay response to wind on the 5 day timescale typical of wind events in Conception and Trinity Bays.

Next we investigate the effect of adding vertical mixing of momentum and density. For a Prandtl number of 1, the addition of vertical mixing does not greatly affect the model response unless A_m and A_ρ in (3) of the appendix have values approaching 10^{-6} m^2 s^{-3}, corresponding to vertical eddy viscosity/diffusivity of 10^{-2} m^2 s^{-1} for $N^2 = 2 \times 10^{-4}$ s^{-2} (see Figure 2). For a Prandtl number less than 1, the model response after 5 days is not greatly different from that in Figure 8. A Prandtl number greater than 1, implying stronger mixing of momentum than density, has a greater effect, particularly in increasing the horizontal scale associated with the model response [*Yamagata and Philander*, 1985]. Figure 9 shows a case with a Prandtl number of 100 corresponding to choosing A_m and A_ρ equal to 2×10^{-6} m^2 s^{-3} and 2×10^{-8} m^2 s^{-3} respectively. These results should be compared with those in Figure 8. The fields in Figure 9 are quite similar to those obtained with Prandtl number 1 when both A_m and A_ρ are equal to 10^{-6} m^2 s^{-3}, showing that on the 5 day timescale being considered here, it is the vertical mixing of momentum that has the most effect in modifying the response. On much longer timescales (e.g., 20 days), the dependence on Prandtl number is more like that predicted by *Yamagata and Philander* [1985]; that is, the model response is broad and diffusive for a Prandtl number of 100 but is characterized by narrow

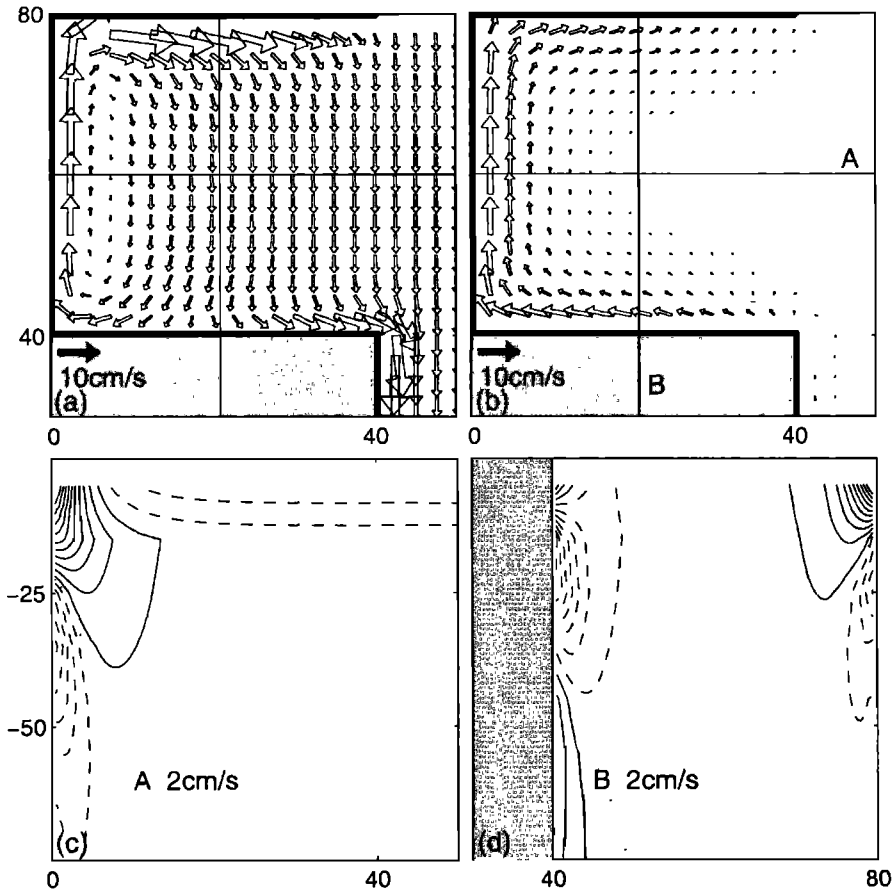

Figure 11. The linearized CANDIE model at day 5 with idealized geometry. (a) Surface level velocity. (b) Second level velocity. (c) Velocity normal to transect A. (d) Velocity normal to transect B. The contour interval is 2 cm s^{-1} with solid lines indicating flow into the page and dashed lines indicating flow out of the page. The dotted lines are the zero contours.

jets, significantly narrower than the radius of deformation for the first baroclinic mode, when Prandtl number equals 0.01.

Implementing the wind stress as a body force acting over a depth of 20 m reduces the importance of the higher modes (as we expect from Figure 7). Figure 10 shows a case with A_m and A_p both set to zero and with H_M =20 m. Note, in particular, that the eastward jet on the south side of the bay near the mouth is weaker than in Figure 8.

4. CANDIE Model

4.1. Linearized Model Runs

In this section we study the response of a flat-bottomec idealized bay to wind forcing using the CANDIE model [*Sheng et al.*, 1998]. We use the idealized model geometry shown in Figure 4 with a uniform depth of 200 m, vertical resolution of 10 m, and horizontal resolution of 500 m. In most of the model runs, vertical viscosity and diffusivity are set at 10^{-4} m^2 s^{-1}, and the coefficients for horizontal mixing of momentum and density are set at 10 m^2 s^{-1}. The density stratification is representative of June, as discussed in Section 2, and identical to that used in the continuously stratified case runs described in Section 3. The density equation is linearized about the (horizontaly uniform) June density profile, and the momentum equations are linearized about a state of rest, although some fully nonlinear runs are described later. The rigid lid, Boussinesq, and hydrostatic approximations are used in the model. The open boundary conditions are described in the appendix and mimic those applied to the shallow water equation models. The model has been tested using vertical viscosity and diffusivity set inversely proportional to N^2, as in the normal mode model. The model results are almost identical to the normal mode solution obtained in Section 3.

As before, a westward wind stress of 0.05 Pa is applied and ramped over 2 days. The zero in time is taken to be 1 day into the ramping. Given that the vertical grid spacing is 10 m, the wind stress is in effect implemented as a body force acting over the 10 m depth of the top model level. Figures 11 and 12 show plots of velocity and density 5 days into the model run. At the head of the bay, the characteristic northward surface jet

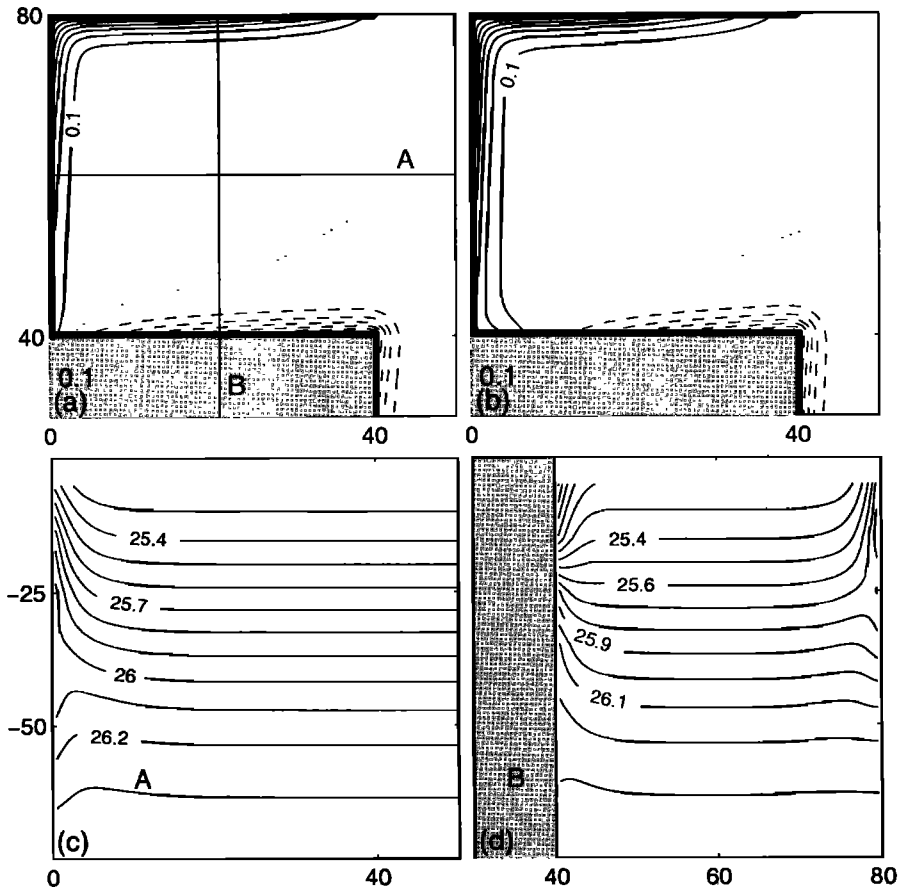

Figure 12. As in Figure 11, but for the density field. Contours intervals are 0.1 kg m^{-3}. Horizontal contour plots are of density departure from initial values. Solid lines indicate denser water, and dashed lines indicate lighter water. Vertical sections are contours of σ_t.

with velocities 10-15 cm s^{-1}, broadens at 15 m depth (Figure 11) and is accompanied by reversal in flow at greater depth, very similar to what was obtained using the normal mode model (Figure 8). At level 2 (15 m depth), the horizontal flow field resembles that obtained using the first baroclinic mode alone. This is a consequence of the vertical structure of the higher modes which have zero crossings at roughly 15 m depth (Figure 3) and thus have little influence on flow at 15 m. At level 2 there is little Ekman driven contribution to the flow. On the southern boundary at the mouth of the bay, the flow at 15 m depth is the reverse of that at the surface (this is also a feature of the normal mode model, see Figure 8). The importance of higher vertical modes noted when discussing Figure 8 can also be seen in the cross sections of the density field (see Figure 12). Note, for example, the pinching of the isopycnals on the southern boundary near 20 m depth in Figure 12 and the fanning out of the isopycnals near 40 m depth on the western boundary.

4.2. Nonlinear Model Runs

Next we apply the full nonlinear equations of motion to the above problem. We use the CANDIE model without any linearization. Model resolution remains at 500 m in the horizontal and 10 m in the vertical, and the model parameters are the same as for the linearized runs. Convective overturning is included so that when hydrostatic instability occurs, the vertical diffusivity applied to density is increased to a large value. A free slip boundary condition is applied to the velocity field and the normal gradient of density is set to zero on the model boundaries.

Figures 13 and 14 show the results of the nonlinear run at day 5. The most striking difference from the linear case (Figure 11) is the separation from the coast of the jet on the north side of the bay. The separation is associated with the offshore advection of upwelled water by the cross-bay Ekman drift. That can be seen by comparing the surface density field in Figure 14 with that in Figure 12. The presence of upwelled water in the interior of the bay leads to an along-bay pressure gradient that supports the separated jet.

On the south side of the bay (Figure 13, transect B), the alongshore component of flow is much weaker than in the linear case (Figure 11). The transport of density across the bay reduces the cross-shore density gradients, weakening the coastal jet set up by the passage of Kelvin

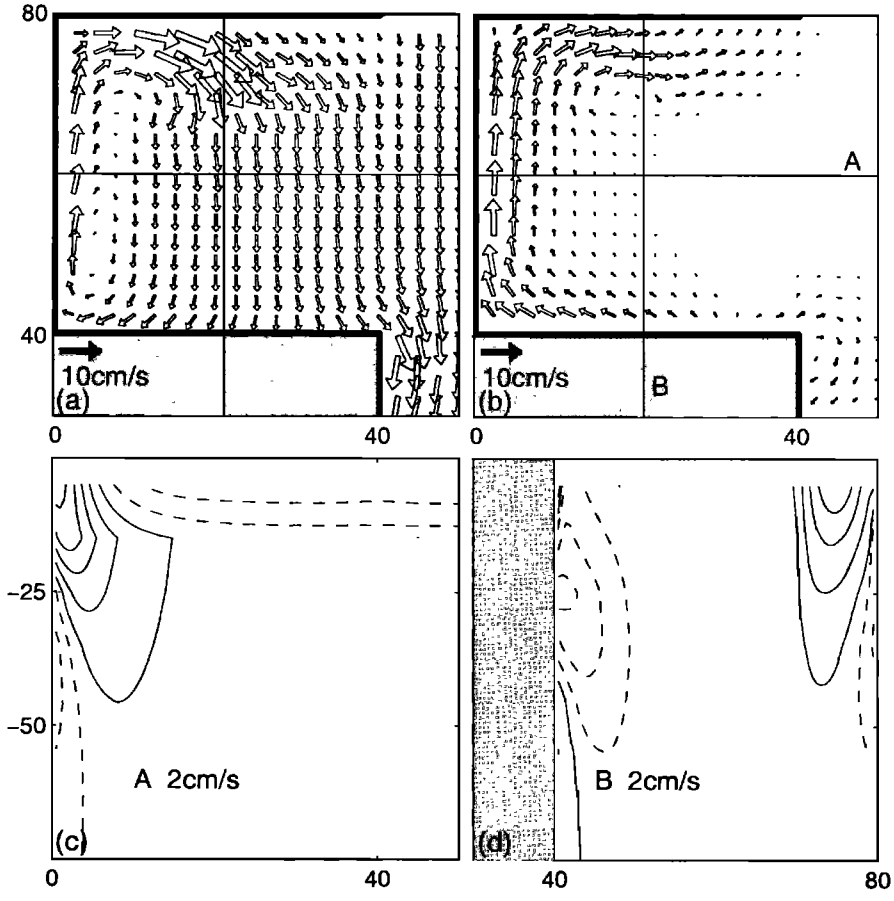

Figure 13. The nonlinear CANDIE model at day 5 with idealized geometry. (a) surface level velocity. (b) second level velocity. (c) velocity normal to transect A. (d) Velocity normal to transect B. The contour interval is 2 cm s^{-1} with solid lines indicating flow into the page and dashed lines indicating flow out of the page. The dotted lines are the zero contours.

waves. Flow in this area is weaker at the surface and at depth. The surface coastal jet on the north side (transect B) extends deeper with the inclusion of the nonlinear terms. Maximum flow strength is ≈5 km off the coast in this crosssection.

At the head of the bay, transect A (Figure 13) shows a weakening of the coastal jet near the coast but a spreading into the interior at depth compared to the linear case (Figure 11). The velocity structure at 15 m depth shows evidence of this broad northward flow. In Figure 14, the density contours on transect A are similar to the linear case with exception of a slight upward displacement of the near surface isopycnals in the center of the bay associated with the cross-bay advection of upwelled water.

The surface density field in the nonlinear case resembles qualitatively the observed surface temperature structure in Figure 1 with a predominantly cross-bay structure and evidence of broad upwelling on the north shore, with upwelled water extending out into the interior of the bay.

5. Models With Realistic Coastline and Bottom Topography

In this section we use the CANDIE model to explore the influence of the realistic coastline and bottom topography of Trinity and Conception Bays (see Figure 5). Since coastal trapped waves travel with the coastline on the right, in the Northern Hemisphere, waves generated in Trinity Bay can influence Conception Bay. Indeed, the influence of Trinity Bay on upwelling events in Conception Bay was inferred by *de Young et al.* [1993] using both a reduced gravity model and observations. Here we investigate the effects of a wind blowing along the axis of the bays (that is at 30° from the x axis of our model domain; see Figure 5). The wind stress has magnitude 0.05 Pa, and as before, it is introduced over a period of 2 days to reduce the excitation of inertial oscillations.

Four different model versions are considered: (1) a single mode for the shallow water normal mode model, (2) the linearized CANDIE model with a flat bottom,

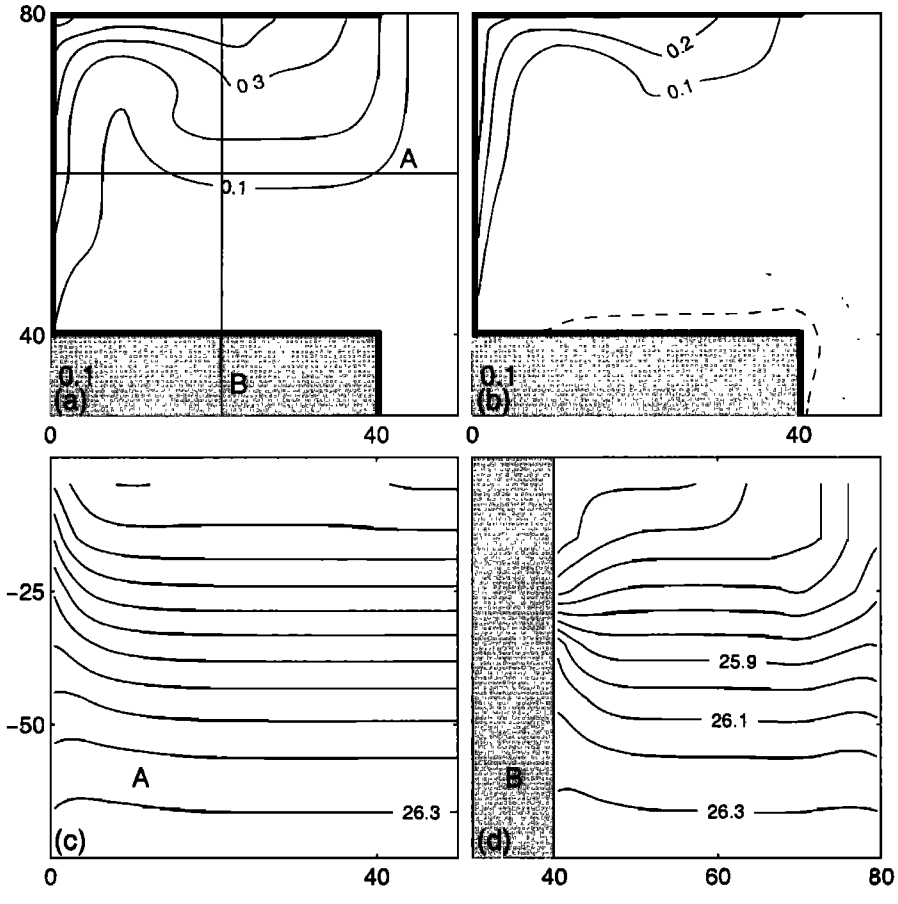

Figure 14. As in Fig. 13 but for the density field. Contours intervals are 0.1 kg m^{-3}.

(3) the linear CANDIE model including realistic bottom topography, and (4) the nonlinear CANDIE model including realistic bottom topography. All models use the same model parameters as in Section 4, apart from the use of 1 km horizontal resolution instead of 500 m to reduce computational cost. A comparison with a 500 m resolution test case indicates good agreement.

Figures 15a-15d show the modeled velocity fields for each of the above mentioned model versions. Figure 15e and 15f show the density field for model versions 3 and 4. Consider model version 1. The first baroclinic mode represents well the initial coastal jet and upwelling on the north shore of Trinity Bay. However, after 5 days, the circulation in Conception Bay is very weak with almost zero pressure gradient across the bay. This lull in circulation in Conception Bay is a consequence of the downwelling Kelvin wave generated on the south side of Trinity Bay compensating for the upwelling wave generated on the north side of Conception Bay. A day later, the circulation builds up again, as the upwelling wave generated in Trinity Bay (on the north side) pushes into Conception Bay.

Moving to continuous stratification (version 2), there is significant flow in Conception Bay, indicative of the role being played by higher-order baroclinic modes. There is also surface flow out of each bay along the southeastern boundary near the mouth, as in the idealized cases (Figure 11), as well as southward coastal jets around the capes and the head of the bays. As in the idealized experiments, the higher modes increase the response time of the bays to wind forcing.

Adding realistic bottom topography (version 3) makes little difference to the model solution on the timescale of 5 days being considered here. We can therefore conclude that in the model solutions, realistic bottom topography is not important for determining the near-surface baroclinic response to wind on a 5 day timescale.

Turning to the nonlinear case (version 4), we see that as in the idealized case (Figure 14), there is cross-bay advection of upwelled water in association with the cross-bay Ekman transport. This leads to the predominantly along-bay structure of the surface isopycnals (Figure 15f), similar to the pattern of isotherms in Figure 1. There is also a suggestion, particularly in Conception Bay, that the coastal jet along the north shore is separating from the coast as in Figure 13. After 10 days of wind forcing (Figure 16), a separated jet is found in both bays and, at even later times (e.g., 16 days, not shown), the flow in both bays is dominated by gyre circulations associated with the separated jets, with two

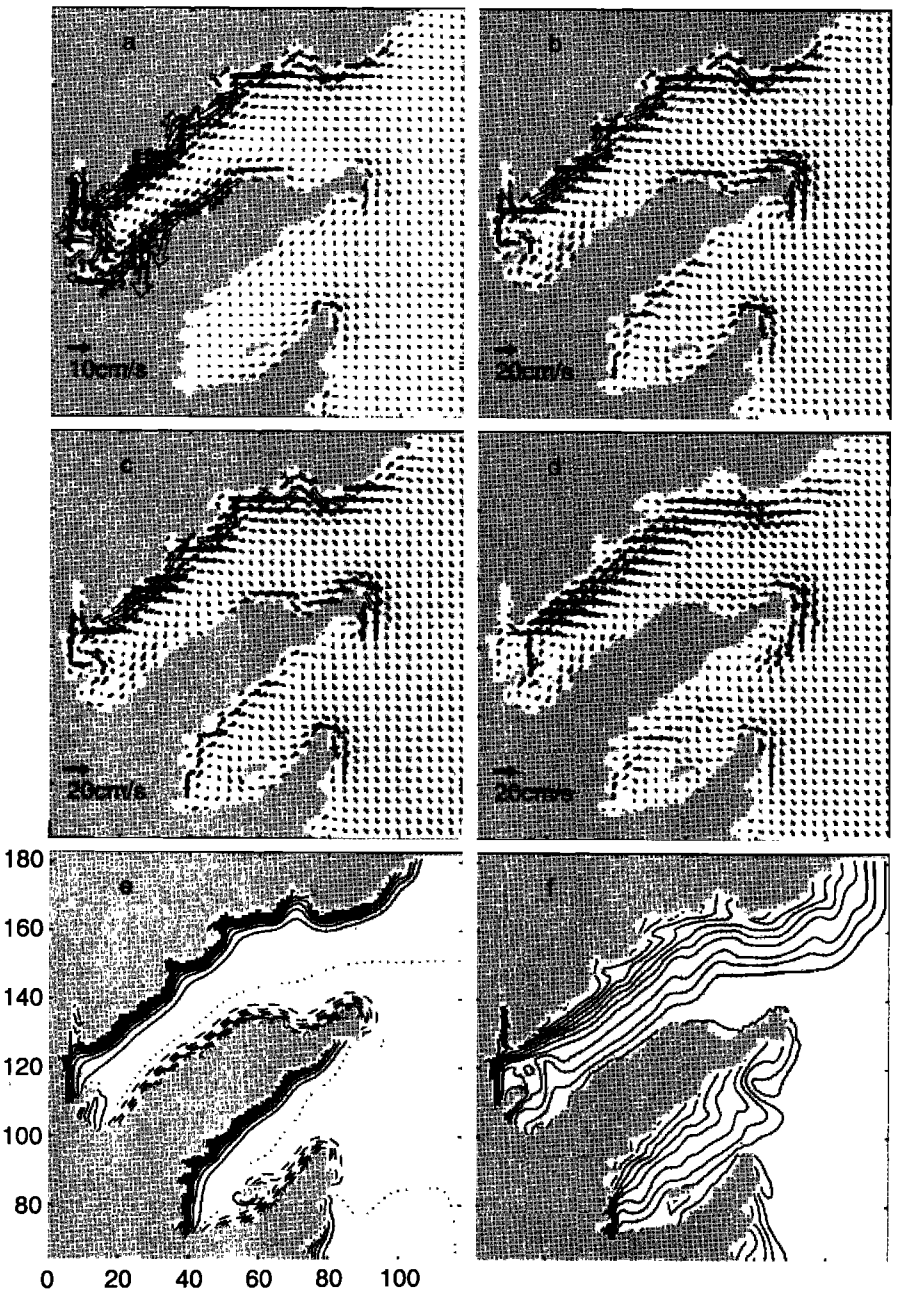

Figure 15. Surface velocities at day 5 from various models with realistic geometry. (a) the single layer, baroclinic model, (b) the linearized CANDIE model with a flat bottom, (c) the linearized CANDIE model with realistic bottom topography, (d) the non-linear CANDIE model with realistic bottom topography. The density departure from initial density for versions 3 and 4 are shown in Figures 15e and 15f, respectively. Solid contours indicate an increase in density, dashed contours indicate a decrease, and the dotted line is the zero contour. Contour intervals are 0.05 kg m^{-3}.

gyres occupying the larger Trinity Bay, as against a single gyre in Conception Bay. These gyres will be the subject of a later study.

6. Conclusion

We have investigated mechanisms that lead to asymmetry in the response of a stratified coastal embayment following the onset of a uniform steady wind that is blowing along the axis and out of the bay. We began with an idealized square bay of 40 km width and a uniform depth of 200 m. Stratification in the bay is representative for June conditions on the east coast of Newfoundland, and the width of the bay is roughly 8 times the first baroclinic Rossby radius. We focus on the 5 day response to steady wind, since 5 days is the

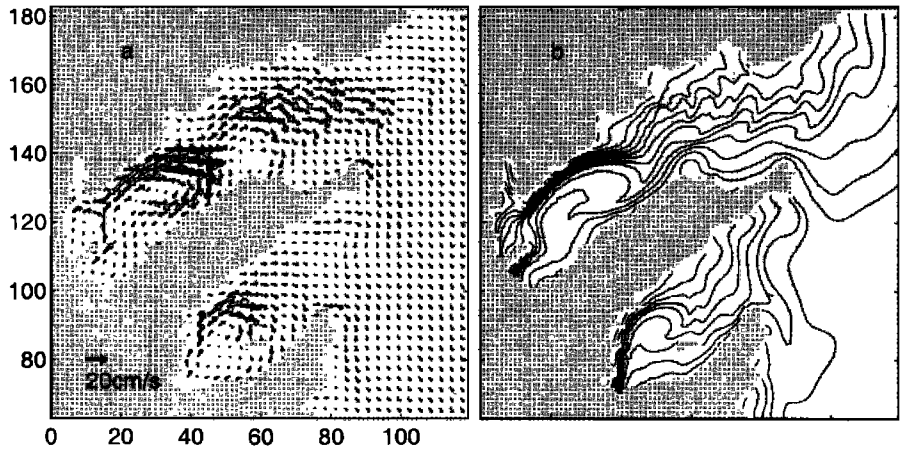

Figure 16. Surface fields at day 10 for the nonlinear CANDIE model: (a) Velocity (b) density departure from initial values with contours of 0.05 kg m^{-3}.

dominant timescale in the wind forcing over Conception Bay [*de Young et al.*, 1993].

If the linear dynamics of only the first baroclinic mode is considered, the response of the idealized bay to 5 days of steady wind forcing is symmetric about the axis of the bay (as noted by *Greatbatch and Otterson* [1991]). The presence of higher modes, with slower wave speeds, breaks the symmetry. Waves associated with mode 3 and higher are still propagating inside the bay after 5 days of wind forcing. The presence of the propagating higher modes leads to an incomplete adjustment and significant asymmetry on the 5 day timescale (see Figure 9). Adding vertical mixing, we found that vertical mixing of momentum, rather than density, is the most efficient at modifying the response on the 5 day timescale, the effect being to broaden the horizontal scales (Figure 10 [*Yamagata and Philander*, 1985]).

Adding nonlinearity allows a significant cross-bay transport of upwelled water and leads to the characteristic along-bay pattern of the surface isotherms evident in Figure 1. The cross-bay advection of upwelled water widens the coastal jet on the upwelling favorable boundary, while it narrows and subdues the coastal jet on the downwelling favorable boundary.

Similar results were found when the realistic coastline and bottom topography of Trinity and Conception Bays were used. Including realistic bottom topography did not significantly change the results on the 5 day timescale considered here. On longer timescales, the nonlinear response of the bays are characterized by gyres associated with the breaking up and separation of the alongshore jet.

Appendix A: Model Description

We describe the three models used in this paper: (1) a single-layer, reduced gravity model, (2) a flat-bottom, continuously stratified model based on the approach of *McCreary* [1981], and (3) the 3-D circulation model known as CANDIE *Sheng et al.* [1998].

A1. Single-Layer, Reduced Gravity Model

The governing equations are

$$u_t - fv = -g'\eta_x + \frac{\tau^x}{\rho_1 H}, \qquad \text{(A1)}$$

$$v_t + fu = -g'\eta_y + \frac{\tau^y}{\rho_1 H},$$

and

$$\eta_t + H(u_x + v_y) = 0. \qquad \text{(A2)}$$

Here, $g' = g(\rho_2 - \rho_1)/\rho_2$ is reduced gravity, f is the Coriolis parameter set at $10^{-4}s^{-1}$, u and v are the velocity components in the x and y directions respectively, and H is the undisturbed depth of the upper layer (here taken to be 40 m) that overlies a deep-resting layer. The response of the model to wind forcing is determined by the wave propagation speed $c = \sqrt{g'H}$, here set at 0.51 m s^{-1} to represent the first baroclinic mode wave speed for June stratification in Conception Bay. The model equations are solved on an Arakawa C grid using the method of *Heaps* [1971].

A2. Stratified Model (Normal Modes)

The 3-D, linearized equations of motion are solved by separation into the standard normal modes for a flat-bottomed ocean following *McCreary* [1981]. The product of vertical viscosity (or diffusivity) times the square of the Brunt Väisälä frequency (N^2) is assumed constant, i.e., $\nu N^2 = A_m$ and $\kappa N^2 = A_\rho$. Here the constants of proportionality A_m and A_ρ can be equal or different, depending on the Prandtl Number, $Pr = A_m/A_\rho$.

We first separate the equations of motion into vertical normal modes and then solve the equations for the hor-

izontal structure of each mode, given below, using the finite difference method of Heaps, as for the reduced gravity model:

$$\begin{aligned}
\frac{\partial u_n}{\partial t} - fv_n &= -\frac{\partial p_n}{\partial x} + F_n - \left(\frac{A_m}{c_n^2}\right) u_n, \\
\frac{\partial v_n}{\partial t} + fu_n &= -\frac{\partial p_n}{\partial y} + G_n - \left(\frac{A_m}{c_n^2}\right) v_n, \qquad \text{(A3)} \\
\frac{\partial p}{\partial t} + c_n^2 \left(\frac{\partial u_n}{\partial x} + \frac{\partial v}{\partial y}\right) &= -\left(\frac{A_\rho}{c_n^2}\right) p_n.
\end{aligned}$$

Here u_n, v_n, p_n, are the velocity components and pressure for each mode. With $\nu = A_m/N_n^2$ and $\kappa = A_\rho/N_n^2$, vertical viscosity and diffusivity appear as Rayleigh friction and Newtonian damping terms in the above shallow water equations. F_n and G_n are the projections of the x and y components of wind stress on each mode and are discussed below. The phase speeds c_n are determined by the normal mode equations and depend on the N^2 profile given to the model (see Figure 2).

It should be noted that the Rayleigh friction and Newtonian damping depends on $1/c_n^2$. Higher modes are damped at a greater rate and, since their phase speeds are lower, have a limited propagation distance before they decay.

We may impart wind stress to the water column either as (1) a body force over a depth H_m or (2) as a surface boundary condition. For the body force implementation, the wind stress projections F_n and G_n are [*Csanady*, 1982]

$$(F_n, G_n) = \frac{(\tau^x, \tau^y)}{\rho_o H_w} \frac{\int_{-H_w}^{0} \phi_n dz}{\int_{-D}^{0} \phi_n^2 dz}. \qquad \text{(A4)}$$

Here τ^x and τ^y are the horizontal components of wind stress, D is the total water depth, ρ_o is the reference density for the model, and ϕ_n is the vertical structure function for the n^{th} mode, normalized so that $\phi_n(0) = 1$.

For wind stress applied as a surface boundary condition, the projections onto the normal modes are given by

$$(F_n, G_n) = \frac{(\tau^x, \tau^y)}{\rho_o \int_{-D}^{0} \phi_n^2 dz}. \qquad \text{(A5)}$$

The model solution is obtained by summing the solutions for (u_n, v_n, p_n) multiplied by the vertical structure function for each mode. The contribution of each mode to the solution is dependent on how wind stress projects onto each mode through the F_n and G_n's (see Figure 7). In all cases, the barotropic mode is not included (in effect, it is assumed that the barotropic velocities are weak and can be neglected; see appendix A3).

A3. The CANDIE Model

We make use of the CANDIE model [*Sheng et al.*, 1998] based on the DieCAST model [*Dietrich et al.*, 1987]. This model solves the 3-D nonlinear Navier Stokes equations on an f plane using the hydrostatic, Boussinesq, and rigid-lid approximations. In the model experiments conducted here, density is used as the model tracer instead of temperature and salinity. The equations are solved on an Arakawa C grid. We use quadratic bottom friction and a free-slip condition on the lateral boundaries. Vertical and horizontal viscosity and diffusivity are set to constant values. We use 10 m vertical resolution throughout the water column. For vertical eddy viscosity of 10^{-4} m^2 s^{-1}, the upper model level contains all of the Ekman transport.

A4. Open Boundary Conditions

The treatment of the open boundaries in the case of the single layer and the normal mode models is the same as by Greatbatch and Otterson [1991]. In particular, the treatment ensures that the model solution knows only about the model domain being considered and that there is no influence (spurious or otherwise) on the model solution from regions outside the model domain. In the case of the 3-D model the treatment is similar, except that the barotropic and baroclinic components of the velocity are treated separately. Along all boundaries, the barotropic component of the velocity is set to zero, thereby ensuring that the barotropic flow within the model domain is weak and can be neglected. This is a reasonable assumption given the small horizontal scale of the region being modeled (as implied, for example, by the arrested topographic wave theory of *Csanady* [1978]). In fact the barotropic pressure adjustment to the wind-forced movement of the surface water is very rapid compared to the baroclinic adjustment we are studying and implies very little vertical averaged flow on the timescale of interest here. As suggested by *Greatbatch and Otterson* [1991], the upstream open boundary (in the sense of Kelvin wave propagation) is an extension of the coastline (see Figure 4). Along this boundary, the normal gradient of both the normal component of baroclinic velocity and the density is set to zero. In the 3-D model, zero gradient conditions are also applied on the other open boundaries and are sufficient to allow propagation of disturbances out of the domain.

Acknowledgments. F.J.M.D. thanks the Federal Department of Oceans, the Maritime Awards Society of Canada and the School of Graduate Studies at Memorial University for financial support in the form of fellowships and scholarships. R.J.G. and B.deY. acknowledge support from NSERC.

References

Crepon, M., C. Richez, and M. Chartier, Effects of coastline geometry on upwelling, *J. Phys. Oceanogr.*, *14*, 1365–1382, 1984.

Csanady, G. T., The arrested topographic wave, *J. Phys. Oceanogr.*, *8*, 47–62, 1978.

Csanady, G. T., *Circulation in the Coastal Ocean*, D. Reidel, Norwell, Mass., 1982.

de Young, B., T. Otterson, and R. J. Greatbatch, The local and nonlocal response of Conception Bay to wind forcing, *J. Phys. Oceanogr.*, *23*, 2636–2649, 1993.

Dietrich, D. E., M. G. Marietta, and B. D. Roache, An ocean modeling system with turbulent boundary layers and topography: Numerical description, *Int. J. Numer. Methods Fluids*, *7*, 833–855, 1987.

Gill, A. E., *Atmosphere-Ocean Dynamics*, Academic,, San Diego,Calif., 1982.

Greatbatch, R. J., and T. Otterson, On the formulation of open boundary conditions at the mouth of a bay, *J. Geophys. Res.*, *96*, 18,431–18,445, 1991.

Heaps, N. S., On the numerical solution of the three-dimensional hydrodynamical equations for tides and storm surges, *Mem. Soc. R. Sci. Liège*, *4*, 143–180, 1971.

Hsieh, W. W., M. K. Davey, and R. C. Wajsowicz, The free Kelvin wave in finite-difference numerical models, *J. Phys. Oceanogr.*, *13*, 1383–1397, 1983.

Killworth, P. D., Coastal upwelling and Kelvin waves with small longshore topography, *J. Phys. Oceanogr.*, *8*, 188–205, 1977.

McCreary, J. P., A linear stratified ocean model of the equatorial undercurrent, *Philos. Trans. R. Soc. London, Ser. A*, *298*, 603–635, 1981.

Petrie, B., J. W. Loder, S. Akenhead, and J. Lazier, Temperature and salinity variations on the eastern Newfoundland shelf: the annual harmonic, *Atmos. Ocean*, *30*, 120–139, 1992.

Pollard, R. T., and R. C. Millard, Comparison between observed and simulated wind-generated inertial oscillations, *Deep Sea Res.*, *17*, 813–821, 1970.

Sheng, J., D. G. Wright, R. J. Greatbatch, and D. E. Dietrich, CANDIE: A new version of the DieCAST ocean circulation model, *J. Atmos. Oceanic Technol.*, *15*, 1414–1432, 1998.

Wilkin, J. L., and D. C. Chapman, Scattering of coastal trapped waves by irregularities in coastline and topography, *J. Phys. Oceanogr.*, *20*, 396–421, 1990.

Yamagata, T., and S. G. H. Philander, The role of damped equatorial waves in the oceanic response to winds, *J. Oceanogr. Soc. Jpn.*, *41*, 345–357, 1985.

F. J. M. Davidson, Laboratoire d'Etudes en Geophysique et Oceanographie Spatiales, CNES/ GRGS/ LEGOS/ UMR5566, 18 Avenue Edouard Belin, 31401 Toulouse Cedex 4, France. (Fraser.Davidson@cnes.fr)

B. deYoung, Department of Physics and Physical Oceanography, Memorial University of Newfoundland, St. John's, Newfoundland, A1B 3X7 Canada. (bdeyoung@physics.mun.cs)

R. J. Greatbatch, Department of Oceanography, Dalhousie University, Halifax, Nova Scotia, B3H 4J1 Canada. (rgreat@phys.ocean.dal.ca)

(Received February 9, 1999; revised August 31, 1999; accepted October 13, 1999.)